Heterogeneously integrated III–V-on-Si laser with embedded photonic molecule mirrors

Guilherme F. M. de Rezende,[1,2,3,*] Newton C. Frateschi,[1,2] and Gunther Roelkens[3]

[1] *Applied Physics Department, Gleb Wataghin Physics Institute, University of Campinas-UNICAMP, 13083-859 Campinas, SP, Brazil*
[2] *Photonics Research Center, University of Campinas, Campinas 13083-859, SP, Brazil*
[3] *Photonics Research Group, INTEC, Ghent University-IMEC, 9052 Ghent, Belgium*
*rezendeg@ifi.unicamp.br

We have designed, fabricated, and characterized a III–V-on-Si laser employing photonic molecule mirrors with high potential for laser tunability and control. Resonant mirrors are realized by tailoring supermodes of coupled microrings. A laser threshold of 40 mA (L-band), series resistance of 10 Ω, and side mode suppression ratio of 40 dB are demonstrated. © 2023 Optica Publishing Group

1. INTRODUCTION, RESULTS, AND ANALYSIS

Coupled optical resonators (CORs) are widely employed in photonics for the investigation of fundamental light–matter interaction as well as in practical telecommunication applications [1] in virtually all integrated photonics platforms. Since they can provide high optical density in a small volume [2], optical resonators have been employed in a variety of applications such as routing [1], multiplexing [3], optical delay lines [4], optical filters [5], signal multi-casting [6], and slow- [7] and fast-light processes [7,8]. For the latter, authors usually apply well-known topological schemes of coupled cavities, the most prominent including coupled-resonator optical waveguides (CROWs) [9] and side-coupled integrated sequence of spaced optical resonators (SCISSORs) [10].

Recently, heterogeneous integration of III–V materials on top of Si based wafers has become one of the most efficient methods to incorporate on-chip lasers sources for a silicon photonics platform [11,12]. Moreover, the variety of techniques developed for its implementation, e.g., divinyl tetramethyl disiloxane-bisbenzocyclobutene (DVS-BCB) (adhesive bonding [13], direct bonding [14], and transfer printing [15]), has led to the successful demonstration of myriad devices relying on both the high optical gain of III–V materials and the low-loss, high-index contrast and small footprint of silicon-on-insulator (SOI) systems [16–19]. In particular, within the context of this work, microring resonators for modal filtering and induced reflection have been reported [20].

In this work, we present a novel design of a III–V-on-Si laser based on DVS-BCB adhesive bonding of III–V materials on a 400 nm SOI e-beam patterned wafer [Fig. 1(a)]. As described below, this design employs photonic molecules for the optical feedback in the laser system. On one hand, when compared to standard cleaved facet mirrors, photonic molecules can be

tailored to present narrow-bandwidth reflection anywhere in the photonic circuit. Therefore, it is a much more powerful element for photonic integrated circuits. On the other hand, compared to other flexible design feedback tools, such as Bragg mirrors or simple resonant structures, photonic molecules have myriad design possibilities that allow tailoring the reflectivity according to each application. Also, they can be widely tunable to cover the entire C + L band (mode-hop included for such tunability). Moreover, photonic molecule alloys employ much smaller areas in the chip since its spectral response depends more on the coupling between molecule resonators than the size of each resonator.

Fabrication follows standard steps as already described in the literature, e.g., [13]. A few fabrication steps will be highlighted and presented with more detail, as needed, in the remaining text. The devices work as follows: light generated in the III–V mesa is coupled back and forth to and from the SOI rib waveguides by means of a double inverted taper [15]. The devices have a symmetric Fabry–Perot (FP) configuration where each mirror is obtained by a system of coupled resonators composed of an outer ring coupled to two embedded rings that are mutually coupled. Figure 1(a) shows a sketch of the proposed idea. When all rings are in resonance, the mutual coupling of this odd number of resonators results in a standing wave supermode due to the breaking of degeneracy between clockwise and counterclockwise bare modes of the microrings [21]. If any of the rings is tuned out of resonance or if a different resonant order is chosen (in which case, the Vernier effect forces detuning between cavities), this phenomenon disappears. Moreover, from the outside reference of a bus waveguide coupled to the outer ring, a degeneracy break appears as an induced reflection that can be tailored according to a compromise between coupling strength and detuning. Interestingly, with proper engineering of the photon lifetime in the outer resonator, one could find
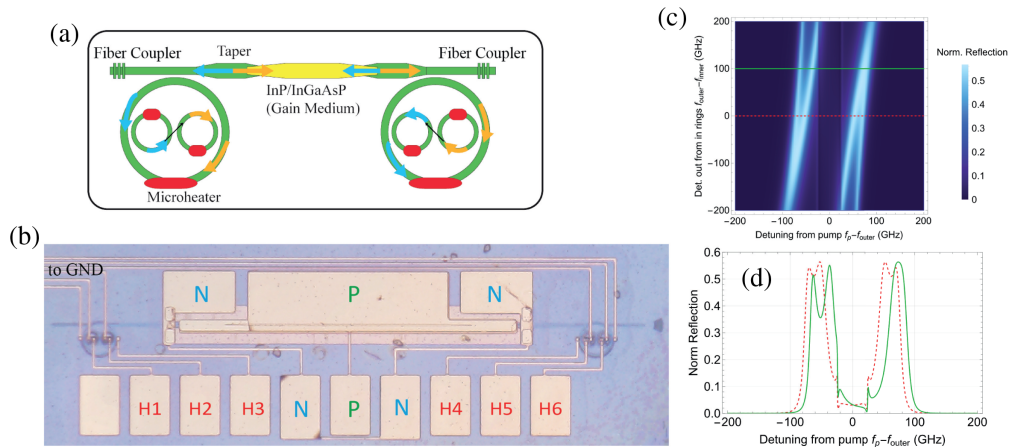
Fig. 1. (a) Schematics of the proposed device. Left to right: grating coupler, photonic molecule with integrated heaters (red) for tunability, and III–V material (yellow). (b) Micro-graph of the fabricated device, highlighting the contact pads. H1–H6, micro-heater pads; N, N-contact, and P, P-contact, of the diode laser. All heaters share a common ground pad (not shown). (c) Simulation of a photonic molecule mirror showing reflectivity (density color) with respect to the degenerated central frequency of the uncoupled resonators in the horizontal axis and detuning of the outer ring resonance in the vertical axis. (d) Simulation of the reflectivity obtained for no-detuning (dashed, red curve) and 100 GHz detuning (solid, green curve) between the outer and two inner ring resonances.

interference of narrow and broad coupled resonances resulting in a Fano reflections and, therefore, a Fano laser [22]. Figure 1(b) shows an optical micro-graph of the fabricated devices where each ring has an integrated Cr:Au micro-heater for tunability. Gold pads allow probing both the diode and the micro-heaters.

The design of the photonic molecule mirror was accomplished employing the transmission matrix method with the improvements of graph theory [23,24] and Mason's gain rule [25]. In our model, the separation of the rings is included in coupling parameter k of a directional coupler that describes the coupling between inner rings or between inner and outer rings. The other important parameters are the complementary transmission, t, related to k such that $t^2 + k^2 = 1$ and the losses for each waveguide section of each ring, or, likewise, the round trip loss of each ring. These parameters are given by: k1 = 0.47 (outer ring to bus coupling); k2 = k3 = 0.345 (outer to inner ring coupling, symmetrical for simplicity); k4 = 0.2 (coupling between inner rings); the round trip losses are: 0.965 for the outer ring (i.e., light completes the round trip with 96.5% of its initial amplitude) and 0.994 for each inner ring. Refractive index dispersion was neglected in this simulation since the wavelength range is relatively narrow. It is important to notice that the coupling between rings is the most important factor to control the reflectivity of the mirror since it controls the coupling between resonator modes, particularly, the coupling between clockwise and counterclockwise modes.

The rings are composed of a 220×650 nm rib waveguide with a 180 nm slab in 400 nm thick SOI platform. The outer ring has a diameter of 40 μm, while inner rings have diameters in such a way that the three gaps between rings vary from 100 to 400 nm in steps of 15 nm. Figure 1(c) shows the calculated reflectivity density plot with respect to the detuning between uncoupled outer ring resonance and laser wavelength in the horizontal axis, and the detuning between outer and inner rings, in the vertical axis. The coupling between ring modes results in a resonance split of approximately 80 GHz centered at

the uncoupled cavities' resonance. At each one of this doublet resonances, one finds the maximum reflectivity when the inner and outer rings are degenerate. Figure 1(d) shows the reflectivity as a function of the detuning between pump wavelength and uncoupled rings, achieved for zero (red) and 100 (green) GHz detuning between inner and outer rings. Reflectivity values near 0.5 are shown to be achievable using this approach. Features of the mirrors obtained by different detunings may be used for controlling laser emission. This is subject to ongoing work, not presented here.

Figure 2 shows schematically a summary of the device fabrication process. The processing flow is as follows: the silicon photonics fabrication has the pattern written onto a SOI wafer by a deep etch lithography process at IMEC (step 1). Both surfaces of the patterned SOI and III–V stack must be very carefully cleaned for a high-quality bond, and, therefore, highly efficient vertical coupling. The bonding is mediated by a solution of 1:8 BCB-mesitylene (1:8) (step 2). Once the bonding is completed, most of the processing follows a standard semiconductor laser process. The SOI layers are insensitive to most of the etchings and processes realized for the III–V stacks. The III–V substrate is removed with a concentrated H2O:HCl (1:3) solution followed by the mesa definition, typically 3 μm wide III–V waveguides with tips tapered down to as narrow as 900 nm by means of 200 nm deposited SiN hard mask (step 3). Subsequently, 200 nm of the InGaAs p-contact layer are etched away by CH4 inductively coupled plasma (ICP) dry-etching. Following that, the thick p-InP layer is anisotropically etched by 1:1 HCl:H2O solution, resulting in an exposition of unetched [111] facets. The wide active layers, consisting of six InGaAsP multiple quantum well (MQW) layers, are dry-etched with the same ICP recipe (step 4). Wet-etching of the n-InP layer into isolated islands is realized. This step employs phosphoric piranha solution and serves for electrically isolating different devices. In our case, since we still must add the metallic heaters
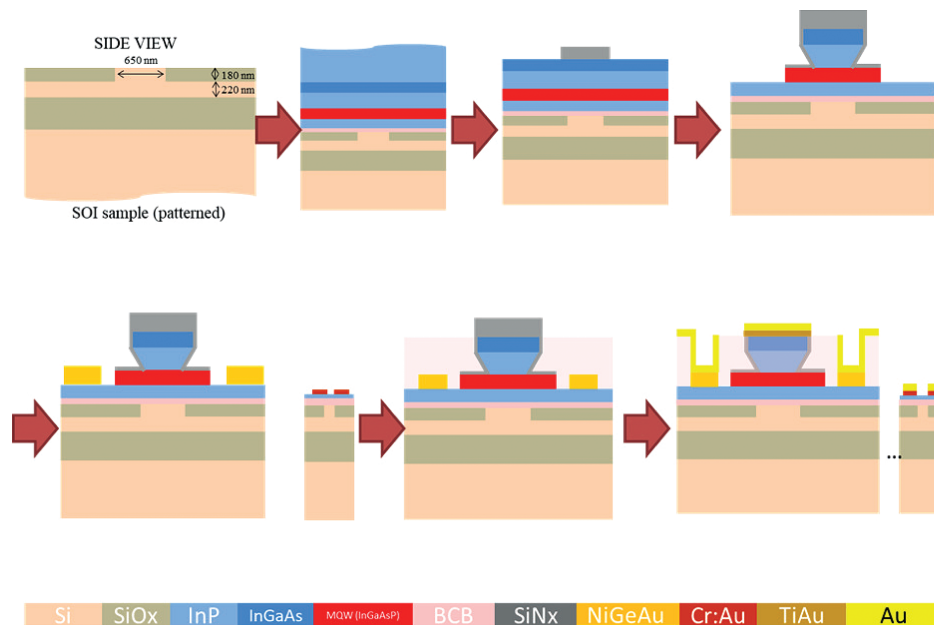
Fig. 2.   Summary of the fabrication steps. Patterned SOI chip coated and cleaved from the foundry (step 1). Both surfaces of the patterned SOI and III–V stack are bonded by a flip chip process with a diluted BCB-mesitylene solution (step 2). Substrate removal and 200 nm deposited SiN hard mask definition (step 3). Mesa definition by means of p-layers (both InGaAs and p-InP) removal; also, wide active region consisting of six InGaAsP MQWs is dry-etched (step 4). N-metallization with Ni:Ge:Au alloy and heater metallization with Cr:Au alloy (step 5). Thick BCB passivation (step 6). Finally, hard mask removal, followed by n-contact metallization (Ti:Au); also, vias are opened in the BCB, and a thick Ti:Au metallization is deposited for electrical contact.

on top of the SOI, this step is essential, but a very thin remaining layer of n-InP is of interest to help with the adhesion of the metallic heater, which is a novel contribution of this work to the original recipe. The n-metallization is deposited by a standard Ni:Ge:Au (30:20:50 nm) alloy. After all epilayers have been etched, we define the metallic heaters on top of the SOI coupled micro-ring mirrors with a Cr:Au (this work), NiCr, or TiAu alloy on top of the remaining InP (step 5). Electrical characterization on separated structures with the heaters shows a resistance of approximately 500 Ω, which corresponds to an electrical power of 8 mW at 2 V (4 mA). We estimate a tunability of 3.6 GHz/mW for 100% efficiency for electrical-to-thermal energy conversion. If all InP is etched, deposition on top of the BCB layer is still possible, but adhesion is very compromised. A thick BCB-57 passivation layer is deposited, not only to provide a sealed device but also to re-planarize the surface to prepare for an etch-back [reactive ion etching (RIE) etch of O2:SF6; step 6]. Finally, the SiNx hard mask is etched away with a RIE dry-etch of CF4:H2:SF6 (50:4:2) follow by n-contact metallization of Ti:Au (40:150 nm). Vias are opened in the BCB layer to reach the n-contact, and a thick metallization of Ti:Au (40:800 nm) is performed for the electrical contact of all layers to its respective pads. This finalizes the fabrication, and the chip is ready to be wire-bonded if desired.

Figure 3(a) shows the scanning electron micro-graph (SEM) of the cross section of the III–V mesa after etching the active layers. One should notice that when the etching ends adequately at the [111] A facets, the mesa is narrower at the bottom. This helps both the process of establishing contact on the top of the mesa as well as improving the optical interaction with the active region—quantum wells. An optical micro-graph of one of the

mirrors is shown in Fig. 3(b). In this case, the outer ring has a radius of 40 µm, while the two inner ones have equal diameters of 38.3 µm and to-outer-ring-gap of 670 nm. Another example is shown in the SEM image of Fig. 3(c), with details on the 187.5 nm gap for the inner-to-inner ring gap. It is interesting to show that the mirrors can be characterized in the middle of the device process, prior to bonding. The transmission shown in Fig. 3(d) is a result of a single-pass transmission through both mirrors. The highest extinction ratio (>20 dB) provides a hint of the spectral region closest to critical coupling from the coupled rings' resonance, which determines the main mode of the cavity. The actual reflectivity spectrum was not possible to obtain from this experiment. Notice that, since the coupling from the rib to slab waveguide in the SOI is lossy (since its tapers are optimized for III–V coupling), a very low transmission of -50 dB is detected. It is important to point out that the observed low transmission power in this measurement is not an issue since the tapers are not optimized for the rib to slab transition in the SOI; rather, we expect optimal coupling to the III–V waveguide after bonding. The measurement using light that couples from the rib to the slab waveguide is performed only to qualitatively check the transmission spectrum of the coupled cavities during fabrication. Also, one should notice that the observed spectrum is a simple product of the transmission of each mirror, and further terms coming from FP effects in the cavity can be neglected at this point. Therefore, qualitative evaluation of the mirrors can be realized. More details could be extracted from the passive structure depending upon the application. Nevertheless, even this simple inspection saves time and material in the very initial step of fabrication, providing valuable information, particularly for manufacturing.
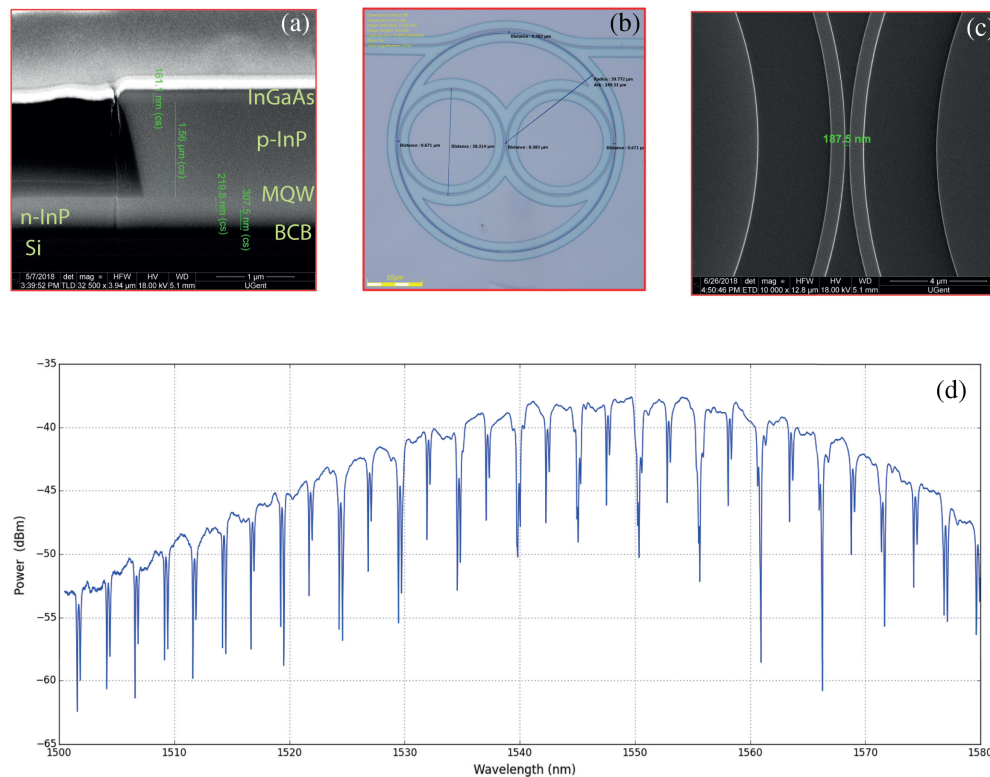
Fig. 3. (a) Scanning electron micro-graph (SEM) image of the cross section of the III–V material after etching of the active layers. (b) Optical microscopy of one of the mirrors showing outer ring (radius of 40 μm and two inner with diameter 38.3 μm and to-outer-ring-gap of 670 nm. (c) SEM image of the inner ring gap; in this case, as narrow as 187.5 nm is achieved. (d) Transmission spectrum of the standalone SOI chip prior to bonding. Light is coupled in and out through grating couplers. Two high extinction ratio (>15 dB) transmissions between 560 and 1570 nm lead to good reflection where typical Q-factors of 10,000s can be achieved.

The fabricated device is shown in Fig. 1(b), where multiple pads drive electrical current in both the laser and heaters. The gain section length is 1 mm, and the FP cavity has a round trip of 2.2 mm (rings are considered part of the mirror and do not count for the FP round trip). The outer ring radius is 40 μm, and the two inner have diameters of 19.1 μm; the outer-to-bus-gap is 200.0 nm, and the inner ring gap and inner-to-outer-ring gap are 187.5 nm.

A series resistance of 10 Ω is observed from asymptotic behavior under higher applied voltages in the IxV measurements during basic laser characterization [Fig. 4(a)]. Considering the IxV behavior measured for the device, it seems that it reasonably deviates from an ideal diode. We consider that its slightly higher series resistance of 10 Ω may cause this deviation. The laser threshold occurs at 1.5 V voltage bias, i.e., a current of 40 mA through the junction, as shown in the light power versus current (LxI) plot in Fig. 4(b). The measured low-output power per facet is primarily caused by output coupling losses. The diffraction grating has coupling losses of the order of 5 dB, which is added by fiber and connector losses to the power meter. Moreover, the design at this stage is optimized to allow lasing and tunability. Therefore, both mirrors have high reflectivity for the passive device, resulting in low external efficiency. Also, the light output from the device was collected by an on-chip grating coupler directly to a fiber and, subsequently, to an optical spectrum analyzer (OSA). A typical laser spectrum is shown in Fig. 4(c)

for several driving voltages where clear notches corresponding to the 2.5 nm free spectral range of the mirror resonances are observed. Voltages are around 1.22 V (20 mA), which is well below the laser threshold. Under this condition, the mirrors accumulate optical energy from the spontaneous emission of the III–V gain region. As voltage is increased, a feedback action is observed, and bumps in the spectrum are observed near the notches. At near 1.6 V (45 mA), the onset of multi-mode laser action is observed at 1566 and 1571 nm. Further increase in voltage suppresses the short wavelength to result in a single-mode emission at 1571 nm. A 40 dB side mode suppression ratio (SMSR) is obtained under this condition. Under voltages higher than 1.87 V, corresponding to injection current of approximately 70 mA, the laser mode shows a hopping to the 1566 nm mode. A clear mode hopping kink in the LxI curve is observed under this condition. We attribute this mode hopping to the next lower wavelength super-mode resonance, mainly due to a thermo-optical mismatch due to heat in the inner cavities. Clearly, this effect shows how strong an active mirror mismatch control on laser tunability would be. The investigation of mirror thermal control for tunability was not available for the reported devices and is the subject of current ongoing research.
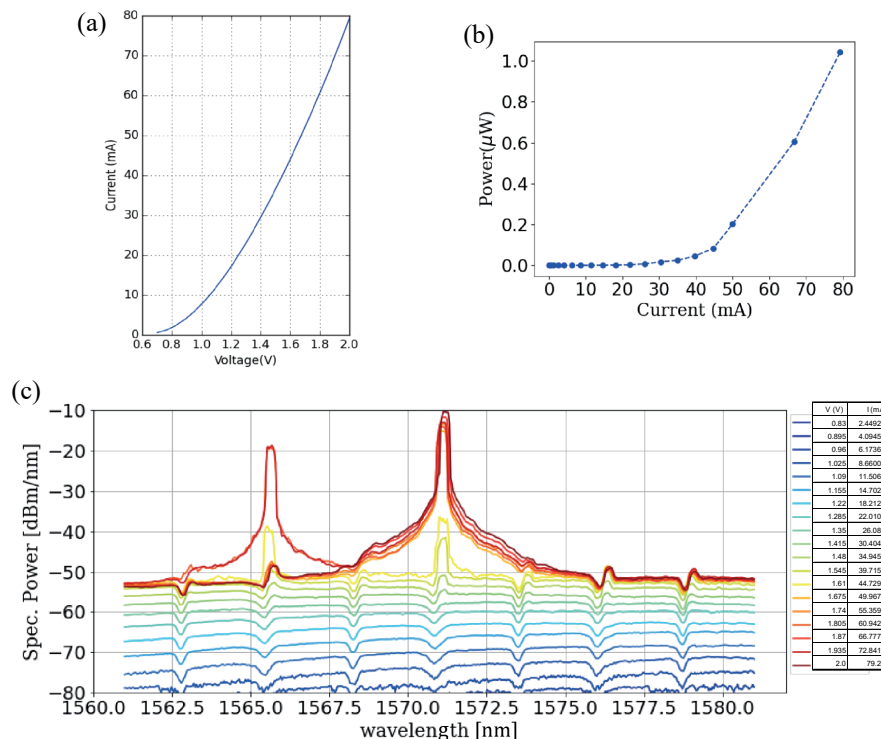
Fig. 4. (a) Junction current–voltage behavior for current values above 1 µA. Under higher applied voltages, a 10 Ω series resistance is extrapolated. (b) Optical power (per facet) for light collected from one grating coupler, showing a threshold current near 40 mA. The dashed line is an aid to the eye. (c) Optical spectrum power density for various voltages across the junction from light collected from the other grating coupler. Laser emits mainly at 1571 nm, with SMSR of 40 dB and mode hopping to 1566 nm for V = 1.87 and 1.95, also observed as a kink in the power output versus current plot.

2. CONCLUSION

In summary, we reported a design, fabrication, and characterization of a novel III–V-on-Si laser employing photonic molecules as resonant mirrors with a threshold of 40 mA and series resistance of 10 Ω. The laser operates in the L-band of the optical wavelengths of telecommunication and presents mode hopping behavior between mirror neighbor resonances separated by a joint free spectral range (FSR). Further investigation is ongoing to reach wide band tunability and mode-hop-free operation.

Disclosures. The authors declare no conflicts of interest.

Data availability. Data underlying the results presented in this paper are not publicly available at this time but may be obtained from the authors upon reasonable request.

REFERENCES

1. W. Bogaerts, P. D. Heyn, T. V. Vaerenbergh, K. D. Vos, S. K. Selvaraja, T. Claes, P. Dumon, P. Bienstman, D. V. Thourhout, and R. Baets, "Silicon microring resonators," Laser Photon. Rev. **6**, 47–73 (2012).
2. L. A. M. Barea, F. Vallini, G. F. M. de Rezende, and N. C. Frateschi, "Spectral engineering with CMOS compatible SOI photonic molecules," IEEE Photon. J. **5**, 2202717 (2013).
3. B. E. Little, S. T. Chu, P. P. Absil, J. V. Hryniewicz, F. G. Johnson, F. Seiferth, D. Gill, V. Van, O. King, and M. Trakalo, "Very high-order microring resonator filters the WDM applications," IEEE Photon. Technol. Lett. **16**, 2263–2265 (2004).
4. J. Cardenas, M. A. Foster, N. Sherwood-Droz, C. B. Poitras, H. L. R. Lira, B. Zhang, A. L. Gaeta, J. B. Khurgin, P. Morton, M. Lipson, R. W. Boyd, D. J. Gauthier, and A. L. Gaeta, "Applications of slow light in telecommunications," Opt. Photon. News **17**(4), 18–23 (2006).
5. B. E. Little, S. T. Chu, H. A. Haus, J. Foresi, and J. Laine, "Microring resonator channel dropping filters," J. Lightwave Technol. **15**, 998–1005 (1997).
6. M. C. M. M. Souza, L. A. M. Barea, F. Vallini, F. M. Guilherme, G. S. Wiederhecker, and N. C. Frateschi, "Embedded coupled microrings with high-finesse and close-spaced resonances for optical signal processing," Opt. Express **22**, 10430–20186 (2014).
7. H.-C. Liu, "Theory and experiment of slow-light coupled-resonator structures," Ph.D. Thesis (California Institute of Technology, 2012).
8. C. Fietz and G. Shvets, "Simultaneous fast and slow light in microring resonators," Opt. Lett. **32**, 3480–3482 (2007).
9. J. K. S. Poon, L. Zhu, G. A. Derose, and A. Yariv, "Transmission and group delay of microring coupled-resonator optical waveguides," Opt. Lett. **31**, 456–458 (2006).
10. X. Tu, L. Y. Mario, and T. Mei, "Coupled Fano resonators," Opt. Express **18**, 18820–18831 (2010).
11. Z. Zhou, B. Yin, and J. Michel, "On-chip light sources for silicon photonics," Light Sci. Appl. **4**, e358 (2015).
12. D. Liang and J. E. Bowers, "Recent progress in lasers on silicon," Nat. Photonics **4**, 511–517 (2010).
13. S. Keyvaninia, S. Verstuyft, L. V. Landschoot, F. Lelarge, G.-H. Duan, S. Messaoudene, J. M. Fedeli, T. D. Vries, B. Smalbrugge, E. J. Geluk, J. Bolk, M. Smit, G. Morthier, D. V. Thourhout, and G. Roelkens, "Heterogeneously integrated III-V/silicon distributed feedback lasers," Opt. Lett. **38**, 5434–5437 (2013).
14. T. Komljenovic, M. Davenport, J. Hulme, A. Y. Liu, C. T. Santis, A. Spott, S. Srinivasan, E. J. Stanton, C. Zhang, and J. E. Bowers, "Heterogeneous silicon photonic integrated circuits," J. Lightwave Technol. **34**, 20–35 (2016).

15. S. Dhoore, S. Uvin, D. Van Thourhout, G. Morthier, and G. Roelkens, "Novel adiabatic tapered couplers for active III–V/SOI devices fabricated through transfer printing," Opt. Express **24**, 12976–12990 (2016).

16. T. Komljenovic, D. Huang, P. Pintus, M. A. Tran, M. L. Davenport, and J. E. Bowers, "Photonic integrated circuits using heterogeneous integration on silicon," Proc. IEEE **106**, 2246–2257 (2018).

17. G.-H. Duan, S. Member, A. Accard, P. Kaspar, G. D. Valicourt, G. Levaufre, N. Girard, A. L. Liepvre, A. Shen, D. Make, C. Jany, K. Ribaud, F. Mallecot, P. Charbonnier, H. Gariah, C. Kopp, and J.-L. Gentner, "New advances on heterogeneous integration of III–V on silicon," J. Lightwave Technol. **33**, 976–983 (2015).

18. J. Hulme, S. Srinivasan, J. E. Bowers, M. Davenport, L. Liang, T. Komljenovic, and R.-L. Chao, "Widely-tunable ring-resonator semiconductor lasers," Appl. Sci. **7**, 732 (2017).

19. Y. D. Koninck, G. Roelkens, and R. Baets, "Design of a hybrid III–V-on-silicon microlaser with resonant cavity mirrors," IEEE Photon. J. **5**, 2700413 (2013).

20. M. A. Tran, D. Huang, J. Guo, T. Komljenovic, P. A. Morton, and J. E. Bowers, "Ring-resonator based widely-tunable narrow-linewidth Si/InP integrated lasers," IEEE J. Sel. Top. Quantum Electron. **26**, 1500514 (2020).

21. M. C. Souza, G. F. Rezende, L. A. Barea, A. A. von Zuben, G. S. Wiederhecker, and N. C. Frateschi, "Spectral engineering with coupled microcavities: active control of resonant mode-splitting," Opt. Lett. **40**, 3332–3335 (2015).

22. M. F. Limonov, M. V. Rybin, A. N. Poddubny, and Y. S. Kivshar, "Fano resonances in photonics," Nat. Photonics **11**, 543–554 (2017).

23. G. F. M. de Rezende, C. M. Kersul, L. A. Barea, G. R. Ascenção, P. L. de Assis, and N. C. Frateschi, "Coupled mode theory revisited: the role of the network topology and ordered directionality," J. Opt. Soc. Am. B **40**, 1005–1016 (2023).

24. G. F. M. de Rezende, "Projeto, caracterização e análise de microrressonadores óticos acoplados em plataforma SOI," M.Sc. dissertation (Universidade Estadual de Campinas, 2013).

25. S. J. Mason, "Feedback theory-further properties of signal flow graphs," Proc. IRE **44**, 920–926 (1956).